

# BUILDING THE PEANUT: SIMULATIONS AND OBSERVATIONS OF PEANUT-SHAPED STRUCTURES AND ANSAE IN FACE-ON DISK GALAXIES

KANAK SAHA

Inter-University Centre for Astronomy and Astrophysics, Pune-411007, India.

ALISTER W. GRAHAM AND ISABEL RODRÍGUEZ-HERRANZ

Centre for Astrophysics and Supercomputing, Swinburne University of Technology, Victoria 3122, Australia.

## Abstract

(X/peanut)-shaped features observed in a significant fraction of disk galaxies are thought to have formed from vertically buckled bars. Despite being three dimensional structures, they are preferentially detected in near edge-on projection. Only a few galaxies are found to have displayed such structures when their disks are relatively face-on - suggesting that either they are generally weak in face-on projection or many may be hidden by the light of their galaxy’s face-on disk.

Here we report on three (collisionless) simulated galaxies displaying peanut-shaped structures when their disks are seen both face-on and edge-on - resembling a three-dimensional peanut or dumbbell. Furthermore, these structures are accompanied by ansae and an outer ring at the end of the bar — as seen in real galaxies such as IC 5240.

The same set of quantitative parameters used to measure peanut structures in real galaxies have been determined for the simulated galaxies, and a broad agreement is found. In addition, the peanut length grows in tandem with the bar, and is a maximum at half the length of the bar. Beyond the cutoff of these peanut structures, towards the end of the bar, we discover a new positive/negative feature in the  $B_6$  radial profile associated with the isophotes of the ansae/ring.

Our simulated, self-gravitating, three-dimensional peanut structures display cylindrical rotation even in the near-face-on disk projection. In addition, we report on a kinematic pinch in the velocity map along the bar minor-axis, matching that seen in the surface density map.

*Keywords:* galaxies: bulges – galaxies: kinematics and dynamics – galaxies: structure – galaxies: evolution – galaxies: spiral, galaxies: halos

## 1. INTRODUCTION

Disk galaxies host “bulges” with diverse morphologies and kinematics. While classical bulges appear rounder, and are somewhat dominated by random stellar motion (although see [Saha et al. \(2012\)](#)), “pseudobulges” may have boxy/peanut-shapes or even display an X-shaped morphology, and they are typically supported by ordered rotational motion ([Combes 2011](#); [Athanasoula 2016](#)). [Buta et al. \(2010\)](#) correctly refers to these latter structures as differing bar morphology rather than bulge morphology. More than 50% of edge-on disk galaxies in the local universe are thought to host these (boxy/peanut)-shaped features ([Bureau & Freeman 1999](#); [Lütticke et al. 2000a,b](#); [Yoshino & Yamauchi 2015](#); [Erwin & Debattista 2017](#)), as does the Milky Way and M31 ([Dwek et al. 1995](#); [Athanasoula & Beaton 2006](#); [Ciambur et al. 2017](#)). It should be noted that the presence of a “pseudobulge”, which is related to the presence of a bar, does not come

at the expense of a classical bulge, which are typically smaller in size. When the disks of galaxies hosting these (X/peanut/bowtie)-shaped features are viewed face-on, these features are thought to appear oval in shape, and have been referred to as “barlenses” ([Laurikainen et al. 2011, 2014](#); [Athanasoula et al. 2015](#); [Laurikainen & Salo 2017](#)).

The pioneering  $N$ -body work by [Combes & Sanders \(1981\)](#), and subsequent studies by [Combes et al. \(1990\)](#); [Raha et al. \(1991\)](#), demonstrated that such peanut structures can be formed via the vertical buckling instability of a stellar bar — such that the inner part of the bar thickens in the vertical direction and when the disk is viewed edge-on, with the bar perpendicular to the line-of-sight, a distinct boxy/peanut, or at times X-shaped, morphology appears. Such a morphological structure has been shown to have drawn its support from an orbital backbone associated with vertical inner Lindblad resonance through which star particles are excited in

the vertical direction, i.e. out of the disk plane (Pfenniger 1985; Pfenniger & Friedli 1991; Patsis et al. 2002; Martínez-Valpuesta et al. 2006). Several  $N$ -body simulations have confirmed this scenario for peanut-shaped structure formation (Pfenniger & Norman 1990; Raha et al. 1991; Athanassoula & Misiriotis 2002; Martínez-Valpuesta & Shlosman 2004; Athanassoula 2005; Debattista et al. 2006; Saha et al. 2013). The association of these peanut structures with bars has additionally been established kinematically (Kuijken & Merrifield 1995; Bureau & Freeman 1999; Chung & Bureau 2004; Debattista et al. 2005; Williams et al. 2011). Even relatively face-on galaxies, e.g. NGC 98 ( $i = 40$  deg), have kinematic signatures of such peanut structures (Méndez-Abreu et al. 2008), and recently Erwin & Debattista (2016) presented further evidence, based on IFU kinematics, of a buckling instability leading to the formation of the boxy/peanut structures previously seen in the somewhat face-on galaxies NGC 3227 ( $i = 48$  deg, Laurikainen et al. (2011)) and NGC 4569 ( $i = 62$  deg, Laurikainen et al. (2004); Jogee et al. (2005)). Collisionless  $N$ -body simulations by Athanassoula & Misiriotis (2002); O’Neill & Dubinski (2003) have shown such peanut structures in face-on projection.

Although not well known, the appearance of such boxy/peanut-shaped structures is *not* limited to the observed edge-on galaxies. That is, galaxies seen with rather face-on disks can also present peanut structures, rather than just oval-shaped barlenses. IC 5240 (Buta 1995), see also Laurikainen et al. (2011), and to a lesser extent IC 4290 (Buta & Crocker 1991, their figure 12 reveals what they identify as boxiness in the inner part of the bar) are two examples, as are NGC 4123 and NGC 4314 (Block et al. 2001), and the *Third Reference Catalogue of Bright Galaxies* (de Vaucouleurs et al. 1991) even contains a (poorly known) discussion of such galaxies. Further examples can be found in Quillen et al. (1997); Laurikainen et al. (2011); Erwin & Debattista (2013). A point of difference to note here is that we do not consider these to just be projections of a 2D bowtie/peanut structure existing in the  $z$ -direction of the galaxy (e.g. Debattista et al. (2005)), but rather are structures in the  $x - y$  disk plane. The identification of these peanut signatures in galaxies with rather face-on disks raises a number of questions regarding their formation as pointed out by Laurikainen et al. (2011) who found nine local galaxies with a thickened peanut-shaped inner bar and disk inclinations less than 65 degrees.

In this paper, we report on the formation of strong peanut structures that are visible in simulations of face-on disk galaxies created using collisionless  $N$ -body simulations and compare these structures with the prototype “face-on peanut” galaxy IC 5240, plus several “edge-on peanuts”. Building on past studies of bar strength,

(e.g. Combes 2016, her figure 4), and following Ciambur & Graham (2016), we provide a quantitative structural analysis of the peanut structures using Fourier harmonics to describe the deviations from pure ellipses of a) the isodensity contours, in the case of the simulations, and b) the surface brightness maps, in the case of the real galaxies. A bar introduces a strong  $m=2$  Fourier mode, while a bar plus a boxy/peanut structure can be represented by an  $m=6$  perturbation (Ciambur & Graham 2016). The strength of this perturbation, and its spatial dimensions, can be measured in the same manner for both simulations and real galaxy images. Having such a set of “peanut parameters” not only enables us to better compare the models with real galaxies, but has the promise of enabling real galaxies to be matched against the evolutionary tracks of simulated galaxies in various parameter scaling diagrams, thereby enabling one to age-date the peanut structures observed in real galaxies.

The rest of the paper is organized as follows: in section 2, we present the setup of the disk galaxy models, explain the ensuing  $N$ -body simulation, and reveal the emergence of the peanut structures which are visible in the face-on orientation of the disks. In section 3, we more fully describe the metrics used to quantify peanut structures. From the Fourier analysis, we present five quantitative measures of the peanut, such as its length and strength (Ciambur & Graham 2016). We then apply this in section 4 to our set of three simulated galaxies, and, for the first time, to a peanut observed in a real galaxy whose disk appears somewhat face-on. In section 5 we compare the structural parameters of both the simulated and real peanuts, and we present the evolution of a simulated galaxy in these parameter scaling diagrams. Section 6 presents the kinematics of the simulated peanut structure, as seen when the host disk is both face-on and edge-on. Finally, a discussion and our primary conclusions are presented in section 7.

## 2. THE SIMULATION

### 2.1. Initial Setup

We present three equilibrium galaxy simulations (Sim1, Sim2 and Sim3), each consisting of an initially axisymmetric disk, a dark matter halo, and a small classical bulge. The initial stellar disk surface density follows an exponential profile along the radial direction, and an approximately  $sech^2(z)$  profile along the vertical direction. The initial dark matter distribution is modeled as a cored halo giving rise to a nearly flat rotation curve in the outer parts (Evans 1993), and the initial bulge is modeled with a cored King profile (King 1966). Each component in the model is constructed using a distribution function (DF, which is a function of integrals of motion, satisfying the collisionless Boltzmann equation)

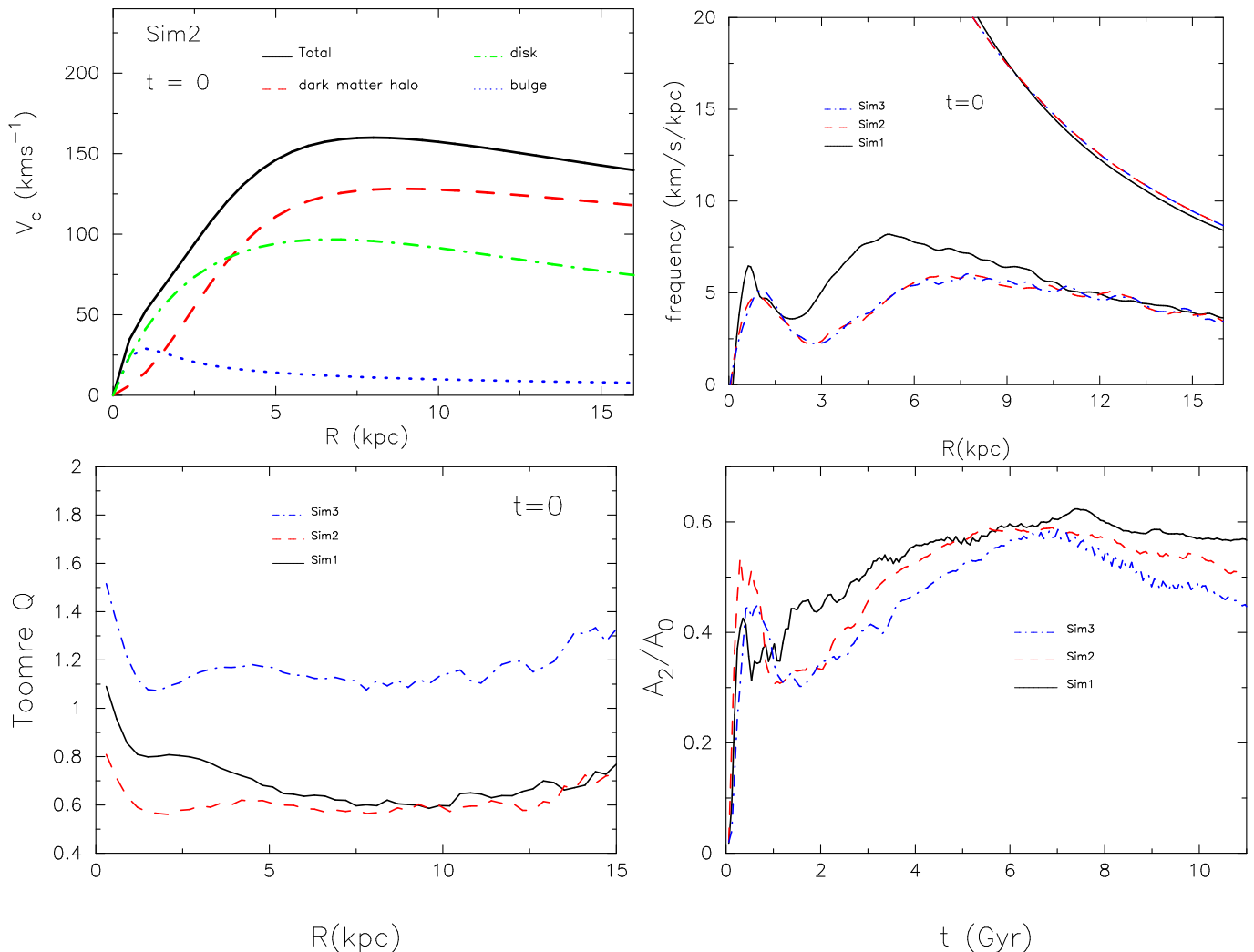


**Figure 1.** Top left: Initial ( $t = 0$ ) circular velocity curves for Sim2. Top right: Initial radial variation of  $\Omega - \kappa/2$  (curves with double humps) and  $\Omega$ . Bottom left: Initial radial variation of Toomre  $Q$  parameter. Bottom right: Time evolution of the bar strength as measured by the maximum of the  $m=2$  Fourier component in the particle distribution.

**Table 1.** Galaxy mass model

Model	$M_{bulge}$ ( $\times 10^{10} M_{\odot}$ )	$M_{disk}$ ( $\times 10^{10} M_{\odot}$ )	$M_{halo}$ ( $\times 10^{10} M_{\odot}$ )	$Q$ ( $R = R_d$ )
Sim1	0.032	1.67	6.8	0.80
Sim2	0.022	1.67	6.5	0.60
Sim3	0.022	1.67	6.5	1.15

$Q$  is the Toomre parameter.  $R_d$  is the initial disk scalelength, equal to 3 kpc.

and are live, allowing them to interact with each other. Further details on the model construction can be found in [Kuijken & Dubinski \(1995\)](#); [Saha et al. \(2012\)](#). The structural properties of the stellar disk are identical in all three models. The mass models differ in terms of their spheroidal components – the bulge and halo component in Sim1 is slightly more massive than those in Sim2 and Sim3, see Table 1.

We have scaled the models such that the initial disk mass  $M_{disk} = 1.67 \times 10^{10} M_{\odot}$ , and the initial disk scalelength  $R_d = 3.0$  kpc. The time between two consecutive snapshots is 60 Myr. Thus, snapshot 0 marks  $t = 0$  and snapshot 200 marks  $t = 200 = 12$  Gyr. The circular velocity curve for Sim2 is shown in Fig.1. The radial variation of  $\Omega - \kappa/2$  for the three models are shown in the top right panel of Fig.1; here,  $\Omega$  is the circular frequency of the stars in the disk, and  $\kappa$  is their radial epicyclic frequency. As combined above,  $\Omega - \kappa/2$  refers to the free precession frequency of an  $m = 2$  mode in the absence of self-gravity and stellar pressure ([Binney & Tremaine 1987](#)). The difference seen here between both Sim2 and Sim3, when compared with Sim1, can be attributed to the different bulge-to-disk mass ratios. The bottom left panel of Fig.1 depicts the initial Toomre  $Q$  variation with radius. Both Sim1 and Sim2 have  $Q < 1$  at nearly all radii, whereas in Sim3  $Q > 1$  at all radii.

We have used a total of 3.7 million particles, with  $0.5 \times 10^6$  in the bulge,  $1.2 \times 10^6$  in the disk, and  $2.0 \times 10^6$  in the dark halo. The masses of the bulge, disk and halo particles are  $451.3M_\odot$ ,  $1.4 \times 10^4M_\odot$  and  $3.1 \times 10^4M_\odot$  respectively. The softening lengths for the disk, bulge and halo particles are chosen following the suggestion of [McMillan & Dehnen \(2007\)](#) for unequal mass particles. The simulations were performed using the Gadget-1 code ([Springel et al. 2001](#)) with a tolerance parameter  $\theta_{tol} = 0.7$ , integration time step (advancing particle coordinates)  $\sim 1.8$  Myr. The simulations were evolved for a total time period of  $\sim 13.2$  Gyr. The total energy is conserved within 2% for the entire run. For Sim1, energy is conserved within 1%. The angular momentum conservation, however, is not good enough for such a long run; the total angular momentum is conserved within 5.0%. We have checked that full system (bulge+disk+halo) is in virial equilibrium with  $T/|W| \sim 0.5$ , ( $T, W$  are total kinetic and potential energy) maintained with deviation  $< 0.1\%$ .

## 2.2. Evolution

The initial axisymmetric stellar disks in Sim1 and Sim2, being cold (with  $Q < 1$  in most of the disk), are subjected to the strongest disk instability due to an axisymmetric mode ( $m = 0$  Fourier mode) [Toomre \(1969\)](#). As a result, the stellar disks undergo fragmentation in the early phase — leading to the formation of stellar clumps which migrate to the center and enrich the pre-existing classical bulge, see [Fig. 2](#), similar to what might be happening in high redshift gas rich galaxies having giant star-forming clumps ([Elmegreen et al. 2008](#)). The migration and coalescence of the stellar clumps in our simulations occur on a rather faster time scale; by about 2 Gyr, most clumps have migrated to the center. The effect of this on the bulge growth can be appreciated visually by inspecting the edge-on images in [Fig. 2](#) at  $t = 0$  and  $t = 1.08$  Gyr. These stellar disks also form short-lived, multi-arm, spiral structures which dissolve, resulting in heating of the stellar disk ([Saha et al. 2010](#); [Sellwood & Carlberg 2014](#)). While the stellar disk in Sim3, being cool (rather than cold), having  $Q > 1$ , does not go through any fragmentation. It evolves by forming multi-arm spiral structures which also end up heating the stars in the disk.

All three stellar disks form a strong bar ( $m = 2$  Fourier component) in the early phase, reaching a peak amplitude of about  $A_2/A_0 \sim 0.5$  within  $t \sim 0.6$  Gyr. The bar amplitude then decays for roughly 1 Gyr, before rising again ([Fig. 1](#)). Note that the initial decay of the bar amplitude is not due to the well-known buckling instability ([Martinez-Valpuesta et al. 2006](#)) but to the fact that those stellar clumps migrate to the center due to dynamical friction from all directions and merge with the

existing bar, leading to a weakening of the bar strength. After this brief period of minimum, the bar starts growing again, and over the next several billion years the stellar disk builds an unusually long bar, especially in Sim1 and Sim2 (with initial  $Q < 1$ ), see [Fig. 2](#).

## 2.3. Emergence of the peanut and ansae

In each simulation, the bar undergoes a buckling instability and forms a boxy/peanut structure which becomes apparent at around 4 Gyr. The strength of this structure increases as time progresses, and it eventually evolves into an X-shaped morphology when seen from the edge-on projection. This boxy/peanut feature is not only visible in the edge-on projection of the disk galaxy (lower panel of [Fig. 2](#)), but also in the face-on projection (upper panel of [Fig. 2](#)). The isophotes of the central region, within about  $1.6 R_d$  (4.8 kpc), are highlighted with the inset images in the top panel of [Fig. 2](#).

Expanding on the previous observation, [Fig. 3](#) clearly reveals the peanut structure at  $t = 12$  Gyr, both in the face-on and edge-on projection, from all three of our simulations — implying that the “peanut” is actually a three-dimensional (3D) structure common to all the models presented here, confirming previous collisionless simulations showing face-on peanuts ([Athanassoula & Misiriotis 2002](#); [O’Neill & Dubinski 2003](#)).

In addition to this boxy/peanut structure, we observe the development of two other structures. In the edge-on view of the galaxy, the peanut extends to larger radii by morphing into a bowtie or X-shaped structure which continues until a certain radial extent, as seen in the X-Z plane. This radial cutoff is associated with the onset of the partial spiral ring or ansae seen at the end of the bar in the face-on projection of the galaxy. Particles/stars at the end of the bar do not exit the disk plane to form the X/Peanut structure, but are instead confined to the disk plane and help to build the ansae/ring.

It remains to be fully investigated what causes such 3D peanut structures. Our simulations do not appear to support a trend of face-on peanut formation with Toomre  $Q$ . Sim3 has a Toomre  $Q$  that is a factor of 2 higher than in Sim1 and Sim2, yet Sim3 still has a similar degree of face-on peanut. We ran an additional simulation with a slightly hotter stellar disk  $Q \sim 1.5$  (cf. 1.15 in Sim 3) and it still formed a 3D peanut. To emphasize that these 3D peanuts are not due to any projection effects, in [Fig. 4](#) we show the density contours from Sim2 taken at four different inclination angles ( $i = 10^\circ, 30^\circ, 50^\circ$  and  $70^\circ$ ), and at 3 different epochs during the evolution. At  $t = 6$  Gyr, there is no sign of a face-on peanut at any of the inclination angles. At  $t = 10.2$  and 12.6 Gyr, the morphology of the contours reveal the presence of a boxy/peanut structure. At lower inclination angles (0 deg being face-on), there is a large-scale bar with a clear pinch along the bar

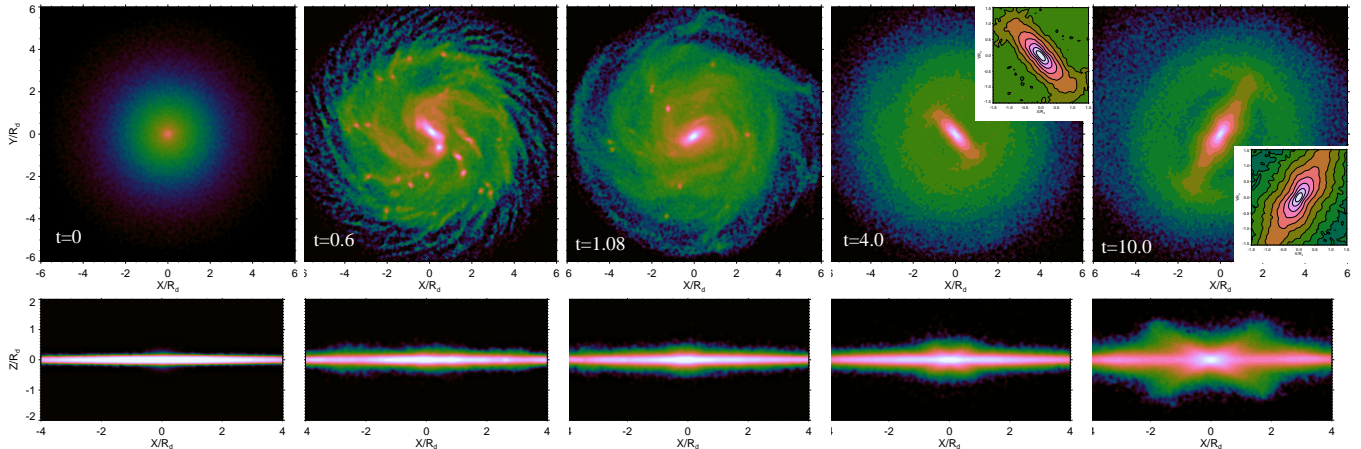


**Figure 2.** Top panel: Face-on surface density maps at different epochs for Sim2. The inset images display the isodensity contours for the inner region of the model. Bottom panel: Edge-on maps at the same epochs. The unit of time is in Gyr.

minor axis, and an associated partial outer ring — an unambiguous signature of a face-on peanut.

In the following sections we quantify these face-on peanut structures, as well as that seen in the galaxy IC 5240.

### 3. QUANTIFYING (FACE-ON) PEANUTS

To the best of our knowledge, peanut structures seen in face-on disks have never been quantified before. We follow the procedure introduced by Ciambur & Graham (2016) to quantitatively describe the properties of peanut-shaped structures seen in edge-on disk galaxies. The distinction here is that we are not measuring a vertical off-plane ( $z$ -direction) feature, but rather an in-plane ( $x - y$ ) feature. The procedure is capable of detecting the existence of peanut features even when they are not very prominent nor the dominant component in the inner region of a galaxy (where they can coexist with the bar, classical bulge and disk). As briefly noted in the Introduction, the technique uses Fourier harmonics to describe the deviations of a galaxy’s isophote from pure ellipses. For a circle of radius  $R$ , the (azimuthal angle)-dependent radius of the quasi-circle is given by

$$R'(\theta) = R + \sum_n [A_n \sin(n\theta) + B_n \cos(n\theta)], \quad (1)$$

where  $\theta$  is the azimuthal angle, and  $n$  is the harmonic order.

While a positive  $m = 2$  cosine harmonic can represent the isophotal perturbation of a bar in a face-on disk, and a negative  $m = 4$  cosine mode can reproduce (boxy/peanut)-shaped isophotes, it is a positive  $m = 6$  cosine mode which captures the combination of a (boxy/peanut)-shaped feature plus a longer bar seen within a face-on disk. This sixth order cosine term introduces six positive and six negative deviations, from

a pure ellipse, as one traverses each ellipse in azimuthal angle (see Figure 5). For a galaxy whose disk is viewed with an edge-on orientation, the six positive deviations match up with the four “prongs” of the peanut structure plus the two “prongs” of the edge-on disk. With either an edge-on disk or a face-on bar contributing positively at an azimuthal angle of 0 and 180 degrees, the positive deviations for the peanut feature would be located at azimuthal angles of  $\alpha = 60^\circ$  above and below the semi-major axis for an isophote with ellipticity  $e = 0$ , i.e. for a circle. If  $e \neq 0$ , these angles are distorted by the quotient of the minor-to-major axis  $b/a$  (see Figure 5).

As one steps out in radius, each quasi-elliptical isophote has its own amplitude of the  $B_6$  term used for quantifying the strength of these deviations. From this radial  $B_6$  profile, one can measure the five parameters defined in section 2 of Ciambur & Graham (2016). Aware that these “peanut parameters” are relatively new in the literature, and therefore likely to be unfamiliar to some readers, we summarize them here.

- (a)  $\Pi_{max}$ : the maximum amplitude of the  $B_6$  coefficient from all radii.
- (b)  $R_{\Pi,max}$ : the radial length of the peanut structure at which  $\Pi_{max}$  occurs, as projected onto the major-axis.
- (c)  $xy_{\Pi,max}$ : the extent of the peanut perpendicular to the bar, but in the disk plane<sup>1</sup>.
- (d)  $S_{\Pi}$ : the ‘strength’ of the peanut, given by the integral between radii at which  $B_6 = \Pi_{max}/2$ .
- (e)  $W_{\Pi}$ : the width of the peanut’s  $B_6$  profile, given by the distance between the previous two radii.

Readers may like to refer to Figures 2 and 3 from

<sup>1</sup> Ciambur & Graham (2016) defined a parameter called  $z_{\Pi,max}$  because they studied edge-on disk galaxies for which they computed the vertical extent of the peanut structures. In our analysis, we explore an equivalent metric in the  $xy$  disk plane of the galaxy, as we are examining face-on disk systems.

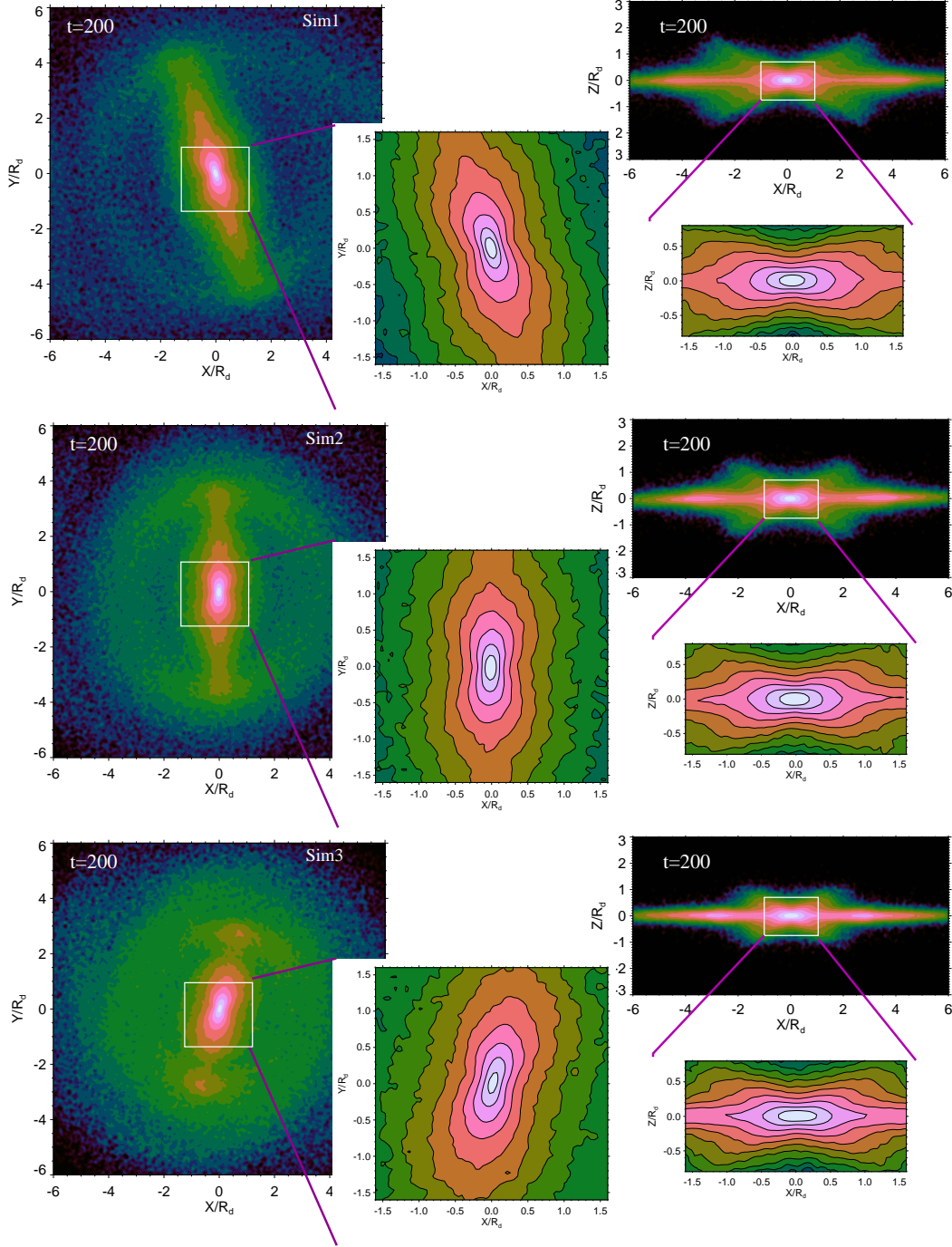


**Figure 3.** Top panels: Sim1 at time step  $t = 200$  (12.0 Gyr). Both a face-on ( $i = 0$  deg) and an edge-on ( $i = 90$  deg) view of the disk reveals the peanut morphology. For the edge-on projection, the major-axis of the bar has been rotated and aligned with the X-axis of the image. The inner  $1.6 R_d$  (4.8 kpc) region shown by the zoomed-in image displays a clear peanut structure in both the Y-X and Z-X plane, while the fainter and more extended (X/bowtie)-shaped structure appears in the Z-X plane. Middle panels: same as above but for Sim2. Bottom panels: same as above but for Sim3. Note: The white boxes in each panel are not to scale, but are purely illustrative.

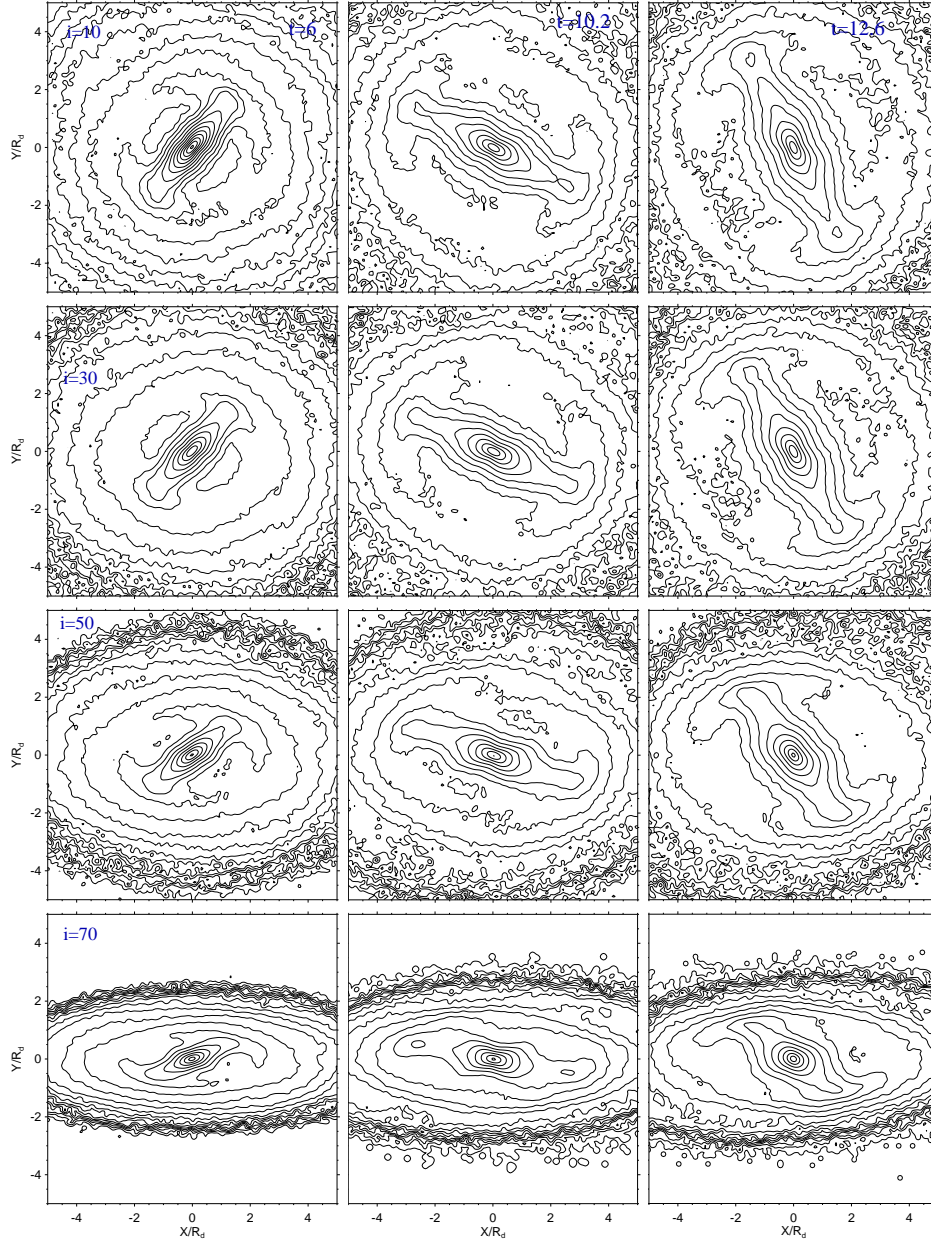


**Figure 4.** Surface density contours for Sim2, projected with different inclination angles, and at three different epochs (6, 10.2 and 12.6 Gyr).

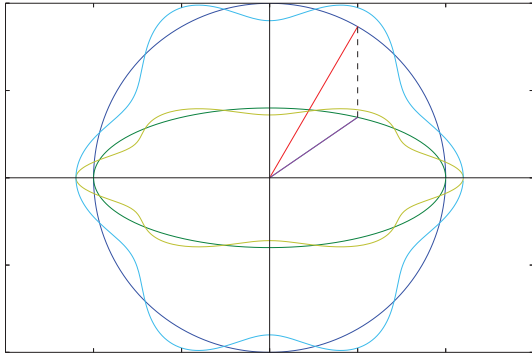


**Figure 5.** The dark green ellipse with ellipticity  $e \equiv 1 - b/a = 0.6$  is distorted using the sixth order cosine term  $B_6 \cos(6\psi)$  of the Fourier harmonic series to create the light green curve. In this example,  $B_6 = 0.1$  has been used. Such a curve is representative of the isophotes of a peanut plus a bar within a face-on disk. The angle  $\psi$  is the eccentric anomaly of the ellipse. In this example, we see how an azimuthal angle  $\theta = 60^\circ$  on the circle, marked by the red line’s departure from the positive X-axis, maps to the reduced angle shown by the purple line. The light blue curve shows the  $B_6 \cos(6\theta)$  deviations.

Ciambur & Graham (2016) for a visual description of these parameters.

Our images were modeled using the new tasks ISOFIT and CMODEL developed for the IRAF software package. ISOFIT was developed by Ciambur (2015) to significantly enhance the modeling of galaxies whose isophotes (or isodensity contours in the case of simulations) depart from elliptical shapes. Taking into account all relevant Fourier terms, ISOFIT varies the intensity of the light in the model to achieve the best match to the 2D light distribution. One can then build a 1-D surface brightness profile along the major-axis,  $\mu(R_{\text{maj}})$ , that includes all of these deviations from a pure ellipse. ISOFIT provides the radial profile of the harmonic terms necessary to do this.

We performed a decomposition of the extracted, major-axis, surface brightness profiles using PROFILER (Ciambur 2016), enabling us to quantify the different constituents of which the systems are composed. For our investigation of the surface brightness profile, the primary component for the analysis is the disk and its inferred scale-length. This is employed to normalize the previous “peanut parameters” in order to perform a fair comparison among different systems, regardless of their distance or size. This decomposition additionally allows us to determine how the length of the peanut, determined by the  $B_6$  profile, correlates with the length of the bar, determined from the surface brightness profile.

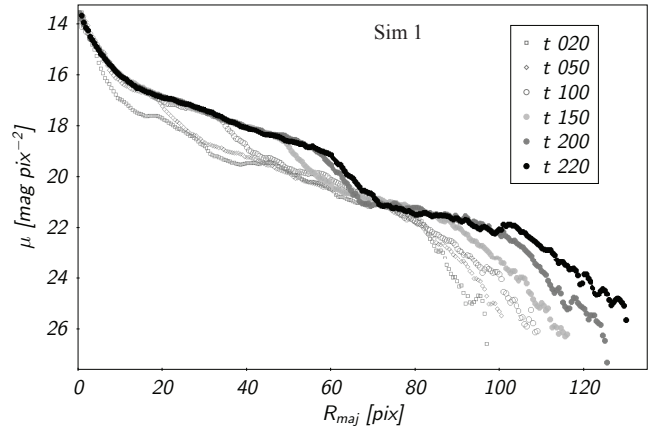


**Figure 6.** Major-axis surface brightness profiles for Sim1, shown at six time steps:  $t = 20, 50, 100, 150, 200, 220$ . A single time step  $\Delta t = 1$  equals 60 Myr. The growth of the bar can readily be seen after  $t = 20$  (1.2 Gyr). For all simulations: 1 pix=1 arcsec=0.234 kpc.

#### 4. APPLICATION

In this section, we will analyze the face-on projections of the three different simulated galaxies, and the real galaxy IC 5240 ( $i_{\text{disk}} = 49^\circ$ , where  $0^\circ$  refers to the face-on view). Unfortunately, we found that our method struggled to model the edge-on projections of the simulations because the X-shaped features do not lie at the appropriate azimuthal angles, and the spikes of the X-shape were too narrow, to be properly captured using Fourier harmonics. This prevented us from obtaining a clean run of the  $B_6$  profile. However, as our investigation pertains to face-on peanuts, our focus was on the face-on projections and we were able to model these well.

For the galaxy IC 5240, we will analyze a  $3.6 \mu\text{m}$  Spitzer image (Sheth et al. 2010). While modeling the surface brightness profile, the fitted model components were convolved with the Point Spread Function (PSF), which was estimated with the IRAF task imexamine by fitting a Moffat profile to 10 stars in the field.

The simulated and real galaxy in our sample do not exhibit a single continuous ellipticity profile,  $\epsilon(R)$ , but instead possess an abrupt transition/jump from high to low values of ellipticity once the bar ends and the ring appears. Thus, we ran ISOFIT two consecutive times. First, for the inner region, we let all the parameters (ellipticity, position angle, and center coordinates) free. Second, from the end of the bar to the outskirts of the galaxy, we fixed the position angle to that of the bar. The best solution for all the galaxies is obtained by using Fourier terms 2, 3, 4, 6, 8, and 10 in ISOFIT. A discussion of the  $m = 8$  mode is beyond the scope of this study, but shall be presented in a forthcoming paper, while a physical meaning for the (very weak)  $m = 10$  mode remains elusive.

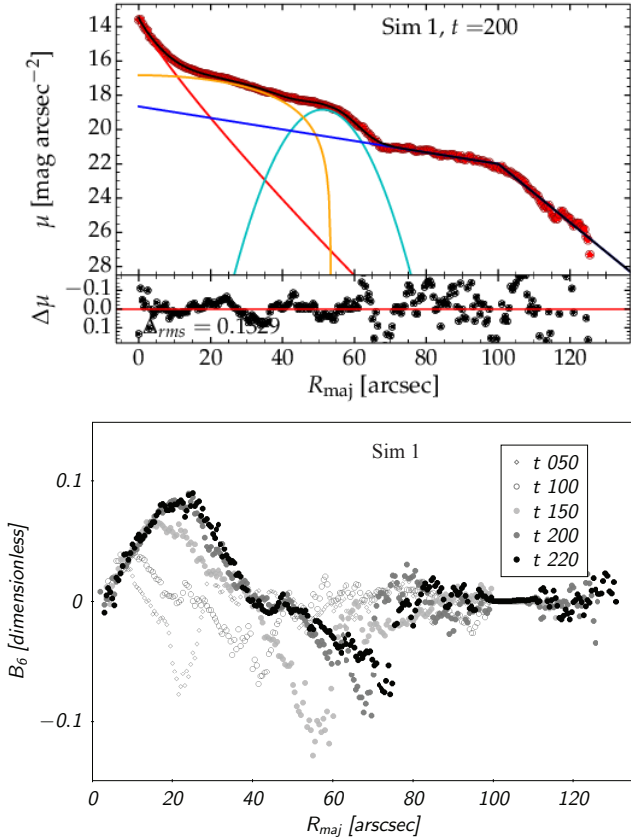


**Figure 7.** Top: Decomposition of the semi-major axis, surface brightness profile of Sim1, when  $t = 200$  (12 Gyr): classical Sèrsic bulge with  $n = 1.2$  (red), broken exponential disk (dark blue), Ferrers bar (orange), and Gaussian ansae/ring (cyan). The radial scale is such that one arcsecond equals one pixel = 0.234 kpc. The inner disk scale-length  $h \approx 32'' \approx 7.5$  kpc. The residual profile of the model subtracted from the data is also shown. Bottom:  $B_6$  radial profiles for simulation 1 at time steps  $t = 50, 100, 150, 200, 220$  (= 13.2 Gyr) show the growth of both the peanut (+ve  $B_6$ ) and the ansae at the end of the bar (small +ve bump then large -ve dip in the  $B_6$  profile).

#### 4.1. The face-on peanut in Sim1

The top panel of Fig. 3 presents our first simulation, at a time step  $t = 200$  (12 Gyr) — the peanut structure is evident in both the edge-on and the face-on projections of the disk. Fig. 6 and 7 reveal the evolution of the bar and associated peanut structure, since its formation at an early age ( $t = 20$  for the bar, and  $t = 50$  for the peanut) until the bar reaches a size of roughly half the stellar disk at 12 Gyr. Figures 6 and 7 display the major-axis surface brightness profile and the  $B_6$  profile, as measured from the face-on orientation of the disk. In Figure 7, the distance from the center of the galaxy, along the major-axis, has been expressed in arcseconds, such that one

**Table 2.** Peanut Parameters: Sim1

time	50	100	150	200	220
$\Pi_{max}$	0.03	0.04	0.07	0.09	0.09
$R_{\Pi,max}$ [kpc]	0.91	1.29	1.94	3.07	3.19
$xy_{\Pi,max}$ [kpc]	0.54	0.70	1.05	1.55	1.62
$S_{\Pi}$ [kpc]	2.13	3.80	12.90	17.0	18.65
$W_{\Pi}$ [kpc]	0.73	1.19	2.48	2.65	2.65

Peanut parameters for Sim1, as seen with a face-on disk, at time steps  $t = 50, 100, 150, 200, 220$  (= 13.2 Gyr), expressed in kpc, except for  $\Pi_{max}$  which is a dimensionless quantity. The inner exponential disk scale-length was found to be fairly constant at  $\approx 7.5$  kpc prior to disk bending/truncation at large radii.

arcsec corresponds to one pixel in the simulation. As the peanut grows with time, the amplitude and width of the associated bump in the  $B_6$  profile can be seen to increase. The negative dips in the  $B_6$  profiles are due to the ansae at the end of the bar. Following section 3, we have computed the five parameters that characterize the “peanutness” of the galaxy using the positive peak in the  $B_6$  profile. The results are gathered in Table 2.

Having quantified the evolution of the peanut in Sim1, we are able to make a number of observations. Over time, the length of the bar grows, as does the radial length where the peanut’s presence is a maximum, as denoted by  $R_{\Pi,max}$ . The ratio of the peanut length to the bar length was observed to remain roughly constant at 0.5 as the bar and peanut co-evolved. The length of the peanut and the bar — relative to the near constant exponential disk scalelength — are thus an indication of the age of these structures in Sim1.

As the bar length and peanut length grow in tandem, the amplitude of the maximum  $B_6$  Fourier cosine term used to identify the peanut, denoted by  $\Pi_{max}$ , was also observed to increase, therefore making it easier to identify the peanut (relative to the background disk) as time increased. Consequently, the bar strength, measured by  $S_{\Pi}$ , also grows stronger with time.

In contrast to the above evolution, the ratio of the peanut’s height relative to its length, i.e.  $xy_{\Pi,max}/R_{\Pi,max}$ , was found to be fairly constant with time, decreasing only slightly from 0.59 at  $t = 50$  to 0.51 at  $t = 220$ . The width of the peanut’s hump in the  $B_6$  profile relative to the length of the peanut, i.e.  $W_{\Pi}/R_{\Pi,max}$  also appears steady at around 0.8 to 0.9 (with the exception of a departure to a ratio of  $\approx 1.3$  at  $t = 150$ ). Therefore, the  $W_{\Pi}/xy_{\Pi,max}$  ratio was also fairly constant at around 0.6–0.75 (with the same exception of the  $t = 150$  snapshot).

In the top panel of Fig. 7, the optimal decomposition of the surface brightness profile of Sim1 at  $t = 200$  (12 Gyr) is shown. It was derived using the PROFILER software (Ciambur 2016). The decomposition consists of an

$n = 1.2$  Sèrsic function to describe the classical bulge, a double exponential function for the disk with an inner scale-length of  $h = 7.5$  kpc, a Ferrers function for the bar and a Gaussian function for the ansae/ring at the end of the bar. The length of the bar at  $\approx 45''$  ( $\approx 10.5$  kpc) is twice the distance where the peanut feature in the  $B_6$  profile is a maximum at  $\approx 23''$  ( $\approx 5.4$  kpc). This same ratio has been observed in real disk galaxies viewed edge-on (Lütticke et al. 2000a; Laurikainen & Salo 2017; Erwin & Debattista 2017).

It should be noted that, along the major-axis, the peanut-shaped structure or “pseudobulge” does not contribute much signal relative to the remaining galaxy light, and is effectively subsumed back into the bar component. That is, there is no additional component required for the peanut in the decomposition. This holds true for all the simulations studied here, and for IC 5240, and also for all of the edge-on galaxies with peanut structures presented in Ciambur & Graham (2016). We suspect that it is highly probable that many past studies of galaxies claiming to have identified and modeled a “pseudobulge” have in fact identified and quantified the classical bulge (which can have Sérsic indices  $n < 2$ ). For a discussion and understanding of this topic, see Graham (2014, 2015).

#### 4.2. The face-on peanuts in Sim2 and Sim3

The top panels in Figures 8 and 9 present the major-axis surface brightness profiles at  $t = 200$  (12 Gyr) for the models Sim2 and Sim3, respectively. These have been fit with galaxy components. Both decompositions consist of a classical Sèrsic bulge ( $n = 0.8$  and  $n = 1.1$ , respectively), a Ferrers bar, a double (or broken) exponential disk, and additional Gaussians that account for the ansae and rings at the end of the bar, features common to barred galaxies (Martinez-Valpuesta et al. 2007).

The bottom panels of Figures 8 and 9 present the  $B_6$  radial profile of each simulation. The first positive bump corresponds to the peanut feature, while the second positive bump together with the negative dip are due to the ansae. As in the previous simulation, the peanut is seen to peak at roughly half the length of the bar. The radius where the maximum of the  $B_6$  peak occurs is close to  $20'' = 4.68$  kpc for Sim2 and about  $15'' = 3.5$  kpc for Sim3, whilst their bars end at  $\sim 9.2$  kpc and  $\sim 6.9$  kpc, respectively.

The maximum amplitude of the  $B_6$  profile from these face-on peanut structures at this time of the evolution are  $\Pi_{max} = 0.09, 0.07$ , and  $0.06$  for Sim1, Sim2 and Sim3 respectively. The peanut parameters derived from the analysis of these two model galaxies are presented in Table 3. What is also apparent from looking at the face-on disk projection in Fig. 3, and from the  $B_6$  profiles in Figs. 7–9, is that a more prominent ansae/pseudo-ring at

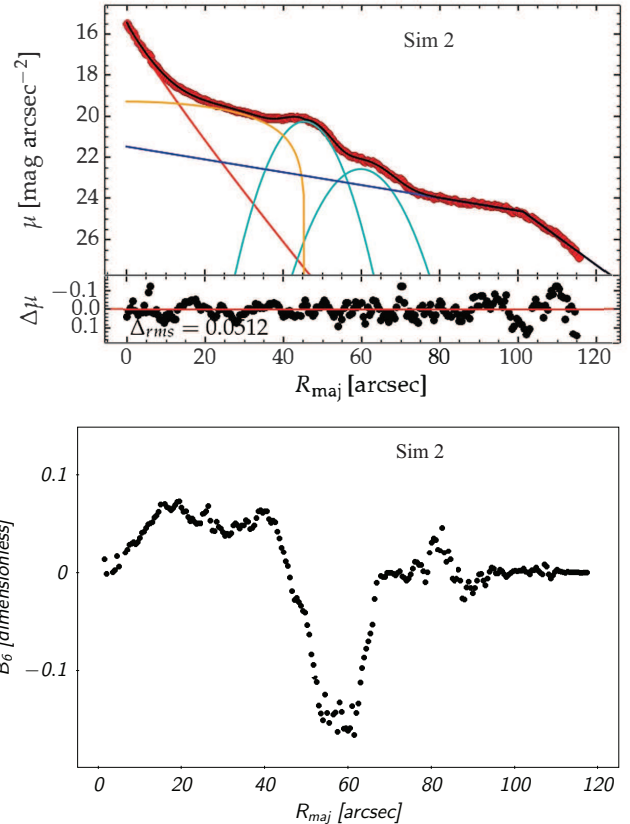


**Figure 8.** Top: Decomposition of the major-axis surface brightness profile, and residual profile (data-model), of Sim2 at  $t = 200$  (12 Gyr), into a classical Sèrsic bulge with  $n = 0.8$  (red line), double exponential disk (dark blue), Ferrers bar (orange), Gaussian ansae at  $\approx 45''$ , and Gaussian ring at  $\approx 60''$  (both in cyan). The radial scale is such that one arcsecond equals one pixel ( $=0.234$  kpc). The inner disk scale-length  $h = 34.9$  arcsec. Bottom: The associated  $B_6$  radial profile. The first positive bump is due to the peanut; the second bump then subsequent dip are due to the ansae.

the end of the bar is associated with a stronger peak in the  $B_6$  profile, which is then followed at larger radii by a negative dip. This will be further investigated elsewhere.

#### 4.3. The face-on peanut in galaxy IC 5240

The same methodology as above has been used here to characterize the peanut in the real galaxy IC 5240. The distance to IC 5240 is  $26.9 \pm 1.9$  Mpc according to NED<sup>2</sup>, based on Planck cosmology (Planck Collaboration et al. 2016), and applying the Virgo, Great Attractor, and Shapley motion corrections Mould et al. (2000) available through NED. For IC 5240, one arcsecond equals 0.13 kpc.

Despite its disk inclination of  $i = 49^\circ$ , we find similar

<sup>2</sup> NASA/IPAC Extragalactic Database: [ned.ipac.caltech.edu](http://ned.ipac.caltech.edu)

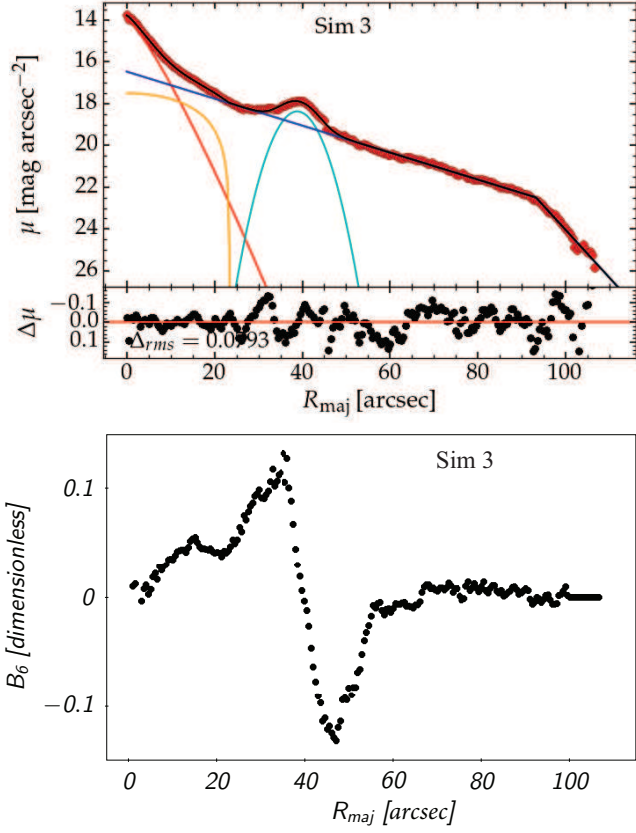


**Figure 9.** Top: Decomposition of the major-axis surface brightness profile, and residual profile (data-model), of Sim3 at  $t = 200$  ( $=12$  Gyr), into a classical Sersic bulge with  $n = 1.1$  (red line), double exponential disk (dark blue), Ferrers bar (orange), and Gaussian ansae. (cyan). The radial scale is such that one arcsecond equals one pixel ( $=0.234$  kpc). Bottom: The associated  $B_6$  radial profile.

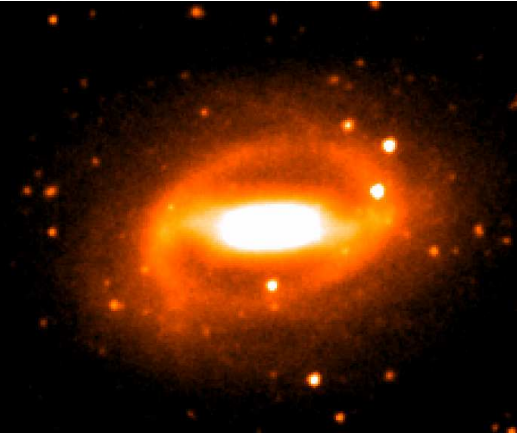


**Figure 10.** Image of the real galaxy IC 5240 observed in  $3.6 \mu\text{m}$  band by the Spitzer Space Telescope.

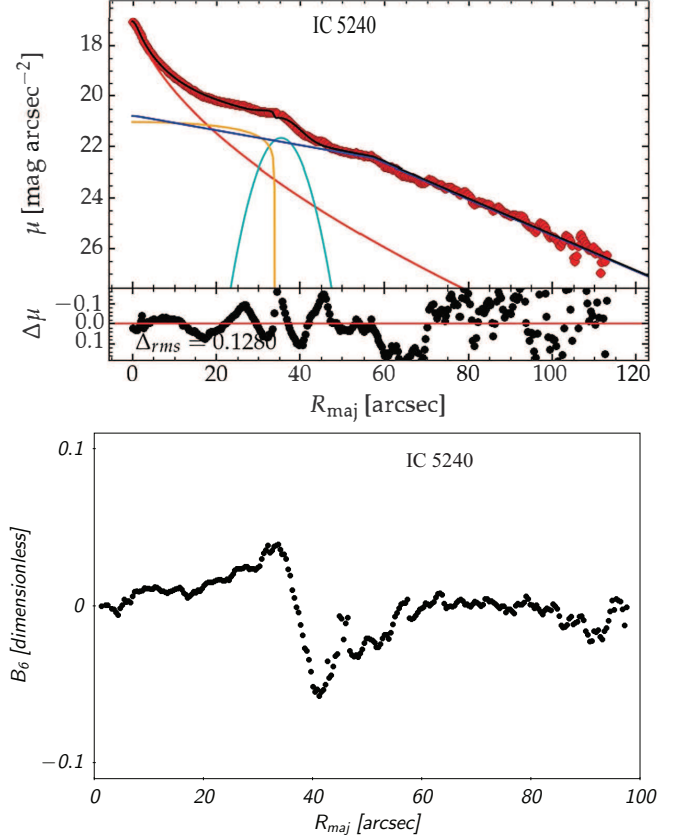


**Figure 11.** Top: Decomposition of the major-axis surface brightness profile, and residual profile (data-model), of galaxy IC 5240 into a classical Sersic bulge with  $n = 1.2$  (red line), double exponential disk (dark blue), Ferrers bar (orange), and Gaussian ansae/ring (cyan). Bottom: The associated  $B_6$  radial profile.  $1'' = 0.13$  kpc.

features in the  $B_6$  profile and the surface brightness profile as to those seen in the simulation. The top panel of Fig. 11 shows the decomposition of the major-axis surface brightness profile of IC 5240, whose constituents are found to be the same as in the simulations: a classical Sersic bulge  $n = 1.2$ , a double exponential disk, a Ferrers bar and a Gaussian ring/ansae. This set of components worked well for all the systems explored.

Similarly, the radial  $B_6$  profile of IC 5240 (bottom panel of Fig. 11) exhibits a positive bump for the peanut with its maximum around  $\approx 15''$  ( $\approx 2$  kpc). The bar in our model ends at a distance of  $\approx 30''$  ( $\approx 3.9$  kpc). The second positive bump in the  $B_6$  profile plus the subsequent dip are due to the ansae/ring at the end of the bar and beyond. The peanut parameters for IC 5240 are included in Table 3.

## 5. PEANUT SCALING DIAGRAMS

We use the new scaling relations for the peanut structures presented in Ciambur & Graham (2016) to compare our simulated 3D peanuts.

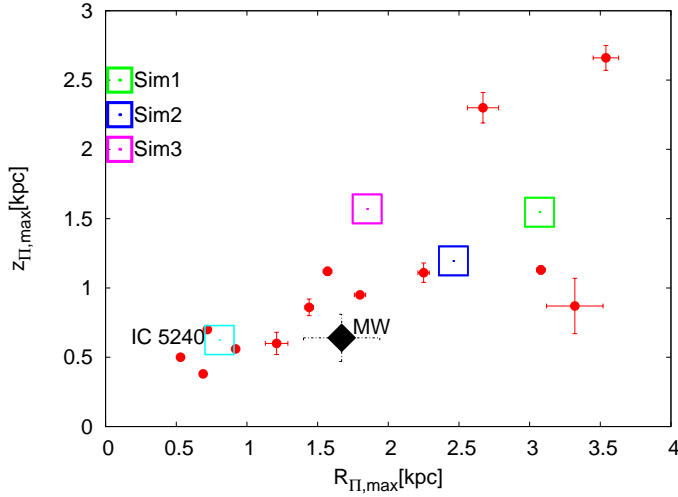


**Figure 12.** Maximum perpendicular departure of peanuts above, and in, the disk plane is plotted against the radial length of the peanut for edge-on disk galaxies (red dots) taken from Ciambur & Graham (2016), and the Milky Way (MW) taken from Ciambur et al. (2017). Over plotted are the face-on peanuts from our simulations and IC 5240. For the face-on peanuts, we have used  $xy_{\Pi,max}$  — the mathematical equivalent to  $z_{\Pi,max}$  (see footnote 1).

**Table 3.** More peanut parameters

	Sim2	Sim3	IC 5240
$\Pi_{max}$	0.073	0.055	0.014
$R_{\Pi,max}$ [kpc]	2.46	1.85	0.80
$xy_{\Pi,max}$ [kpc]	1.19	1.57	0.62
$S_{\Pi}$ [kpc]	13.5	7.07	0.70
$W_{\Pi}$ [kpc]	2.40	1.82	0.67
$h_{disk}$ [kpc]	8.17	3.93	4.8

Quantitative peanut parameters for the evolved ( $t = 200$ , 12 Gyr) galaxy models Sim2 and Sim3, and for the real galaxy IC 5240. The quantity  $h_{disk}$  denotes the inner exponential scale length for the disk in Sim2, Sim3 and IC 5240.

Fig. 12 shows the scaling diagram involving the radial length of a peanut,  $R_{\Pi,max}$ , to its perpendicular departure from the major-axis,  $xy_{\Pi,max}$  (or  $z_{\Pi,max}$ ). Note, this denotes the isodensity contour or isophote where the peanut appears strongest; it is not some fainter contour towards the end of the bar, marking the full extent of the peanut. Parameters for real galaxies, except IC 5240 are taken from Ciambur & Graham (2016) and that of the Milky Way (MW) are from Ciambur et al. (2017). All three simulated peanuts follow the general trend shown by the observed peanuts

In Fig. 13, we compare the integrated strength of our simulated peanuts with their radial extent, along with other galaxies including the MW. For the peanut struc-

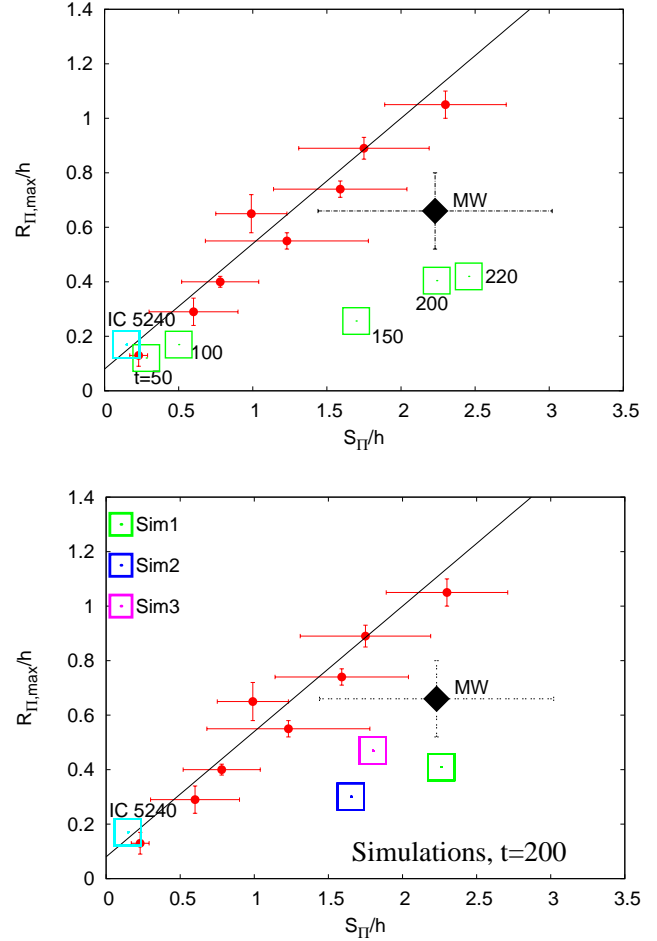


**Figure 13.** Radial length versus integrated strength of the peanut structures seen in galaxies taken from Ciambur & Graham (2016) (red dots). Over plotted on this are our simulated face-on peanuts, IC 5240, and the Milky Way (MW, Ciambur et al. (2017)). Solid line is the linear regression between  $R_{\Pi}$  and  $S_{\Pi}$ , see Ciambur & Graham (2016). Top panel: For Sim1 at  $t=50, 100, 150, 200, 220$ . Bottom panel: simulated peanuts at  $t=200$  (12 Gyr).

tures in galaxies from Ciambur & Graham (2016), there seems to be a linear relation between the strength and length of the peanut: the longer the peanut, the stronger it is. After 12 Gyr, our simulated peanuts (and the Milky Way) seem to deviate from this linear relation defined by the other galaxies. This relation can perhaps now be understood as an age effect. From Sim1, we learned that as the system evolved, the peanut (and bar) gets longer and stronger (see Table 2). In passing, we note that unlike with the simulations, within the sample of real galaxies, the bars are not always viewed perpendicular to the line-of-sight. Consequently, the projected quantities  $R_{\Pi,max}$  and  $W_{\Pi}$ , and thus  $S_{\Pi}$ , will be reduced from their intrinsic value.

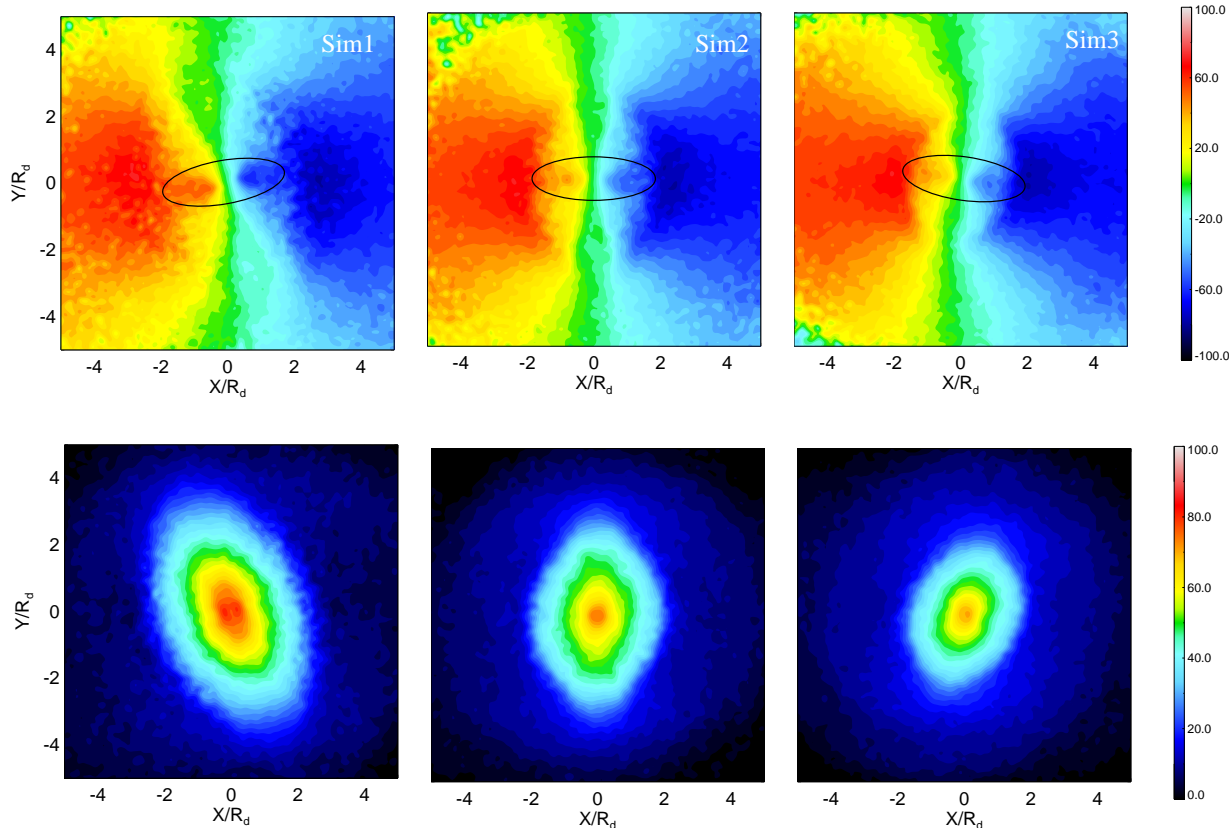


**Figure 14.** Top panel: Line-of-sight velocity maps for all three models, taken at  $t = 200$  (12 Gyr). The models are oriented such that the disk has an angle of  $30^\circ$  from face-on. Bottom panel: Same as above but for the velocity dispersion. A “kinematic pinch” along the bar minor-axis is evident in the velocity map, indicated by the black ellipses. The kinematic maps have the same color bar indicated on the right.

We additionally present the time evolution of the peanut that grows in model Sim1. At  $t = 50$  (3 Gyr) and  $t = 100$  (6 Gyr), the peanut from Sim1 is close to the linear regression followed by other galaxies and IC 5240. As time progresses, the Sim1 peanut gets stronger and eventually its strength becomes comparable to that of the Milky Way’s peanut. Overall, our simulated peanuts are stronger when compared to peanut structures in other galaxies. This is perhaps not surprising given the relative strength of the peanut to the underlying disk, as seen in Figure 3 and traced by  $\Pi_{max}$ . Off the major-axis, Sim1 has contributed much of its disk stars to the bar and peanut (Figure 3), this is less true in Sim3 which resides closest to the line in Figure 13. One of the uncertainties that may affect such a comparison is the orientation of the bar/peanut in the plane of the disk (as mentioned above). Measurements from our simulations are on the higher side (in fact, they are the maximum) as the bar is oriented perpendicular to the line-of-sight. Any deviation from this, would lead to a decrease in the measured values of the parameters defining the peanut structures.

This would apply to all the scaling relations that we use to compare with our simulated peanuts.

In the following section, we discuss the kinematic scaling relations followed by our simulated peanuts.

## 6. KINEMATICS OF FACE-ON PEANUT STRUCTURES

### 6.1. Kinematic pinches

Alongside photometry, the kinematics of galaxies have also played an important role, not only in characterizing boxy/peanut/X-shapes, but also enhancing our understanding of their basic physical nature. A typical such peanut structure would exhibit cylindrical rotation in edge-on projection (where the rotation axis,  $z$ , is perpendicular to the line-of-sight). In that case, the line-of-sight velocity at a given projected radius becomes independent of  $z$ , i.e.,  $dV_{LOS}(X = X_0, z)/dz \simeq 0$ , where  $X = X_0$  is any location within the peanut structure along the major axis. The cylindrical rotation is, therefore, a standard kinematic proxy for a peanut structure, although there are exceptions both in observations and simulated peanut

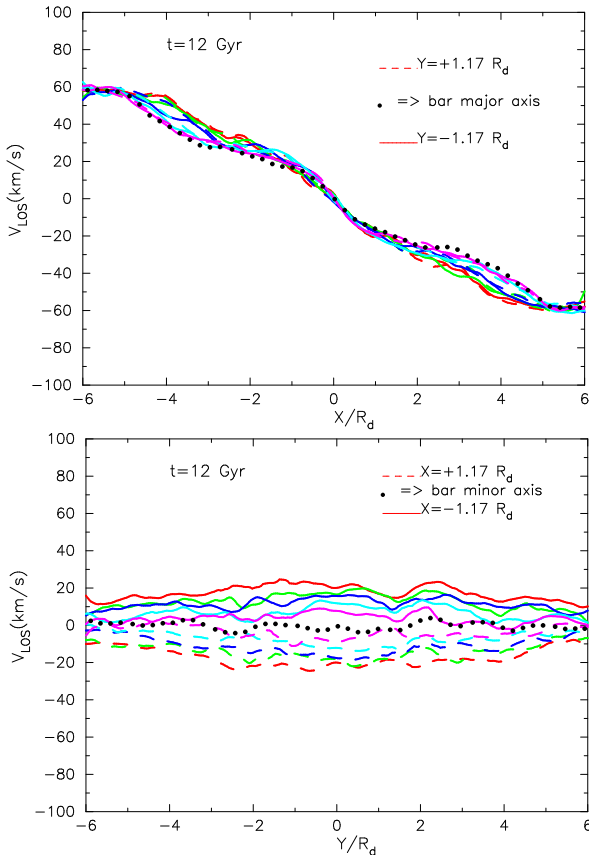


**Figure 15.** Top: Line-of-sight velocity profiles along slits parallel to the bar major axis at  $t = 200$  (12 Gyr) for Sim1. The model’s disk is oriented at an angle of  $30^\circ$  from face-on. Five slits are placed above the bar major axis (positive  $Y$ -values) and five below. The furthest slits are marked in red (solid and dashed lines) at  $Y = \pm 1.17 R_d$  (where  $R_d$  is the initial  $t = 0$  disk scale-length equal to 3 kpc). The distance between two consecutive slits is  $0.24 R_d = 720$  pc. Bottom: Same as above but for the minor axis velocity profiles.

structures (Williams et al. 2011; Saha & Gerhard 2013).

In Fig. 14, we show the 2D line-of-sight velocity and velocity dispersion maps ( $i_{\text{disk}} = 30^\circ$ ) for all three models at  $t = 12$  Gyr; see Fig. 4 for their respective surface density maps. The velocity maps clearly show rotating model galaxies, but their inner parts are rather slowly rotating (although they were not initially). At  $t=12$  Gyr,  $V_{\text{max}}/\sigma_{\text{in}} \simeq 1.5$  for Sim1; 1.7 and 1.9 for Sim2 and Sim3 respectively. Interestingly, these face-on peanuts are associated with a “Kinematic Pinch” along the bar minor axis. We have already identified such a pinch in the surface density maps. The pinch (both photometric and kinematic) is stronger in Sim1, and diminishes gradually in Sim3. When the kinematic maps are available for IC 5240, we would expect to observe such a pinch.

### 6.2. Cylindrical rotation?

In the following, we examine the major and minor axis velocity profiles of the stars in near face-on projection.

The extent of the 3D peanut is about  $1 R_d$ , whereas the outer X-shape extends to more than  $2 R_d$  in edge-on projection, see Fig. 3. The upper panel of Fig. 15 shows the LOS velocity profiles along the major of the bar at  $t = 12$  Gyr for 11 slits placed parallel to the bar major axis. The outer slits are at  $Y = \pm 1.17 R_d$ , basically covering most of the bar along  $Y$ -axis. There is a clear wavy nature in the profiles. We have checked this also at earlier times. At  $t = 4$  Gyr, when the bar still shows no pinching but has formed a boxy structure, the velocity profile shows small scale wavy signature. At later times, such wavy features in the velocity profile become much more prominent.

Apart from the wavy feature, we notice that within about  $X = 2 R_d$ , the velocity profiles are hardly separable, that is, the velocity profiles along the bar minor axis change very little:  $dV_{\text{LOS}}(X < 2R_d, Y)/dY \simeq 0$ . This is exactly analogous to the cylindrical rotation observed in edge-on projection - in other words, these face-on simulated peanuts exhibit cylindrical rotation even when the disk is oriented in such low inclination angle.

In the bottom panel of Fig. 15, the minor axis velocity profiles are displayed along 11 slits placed perpendicular to the bar major axis. The outer most slits are at  $X = 1.17 R_d$  on either side of the bar minor axis. Obviously, the variation of  $V_{\text{LOS}}$  with respect to  $Y$  is insignificant. It turns out that the inner part of the peanut structure (approximately the zoom-in area shown in Fig. 3) exhibit strong cylindrical rotation from high inclination angle ( $i = 90^\circ$ ) to as low as  $30^\circ$ . It turns out that at  $t = 12$  Gyr, the bar pattern speed is  $\Omega_B \simeq 6 \text{ km s}^{-1} \text{ kpc}^{-1}$ , a value very close to the slope  $dV_{\text{LOS}}/dX$  within the inner  $\sim 1.5 R_d$ . Note that all three bars in our simulations showing face-on peanut are indeed slow bars i.e., their corotation to bar length is greater than 1.4.

### 6.3. Kinematic scaling diagram

In Fig. 16, we present a kinematic scaling diagram for our simulated peanuts and compare with those in Ciambur & Graham (2016). We computed  $V/\sigma$  for each of the simulated models at different epochs during the evolution; such that  $V$  is the maximum rotation velocity in the disk and  $\sigma$  is the central velocity dispersion (averaged within a 1.5 kpc region about the center). The quantity  $V/\sigma$  is indicative of how slowly or fast the galaxy (not the peanut) is rotating. Sim1, which formed the strongest bar and strongest peanut, is the slowest rotating galaxy among the models presented here. Fig. 16 shows the variation of  $V/\sigma$  with the length and strength of the simulated peanuts and compared with Milky Way peanut. The simulated peanuts are in broad agreement with the observed peanut kinematic scaling relation. It

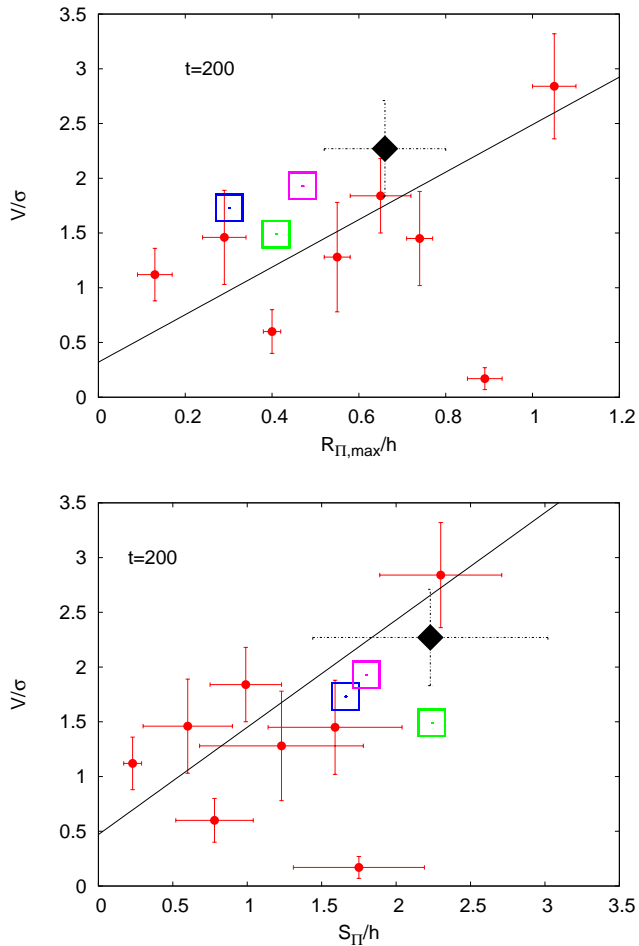


**Figure 16.** The dependence of  $V/\sigma$  on the length and strength of the peanut structures in a sample of edge-on galaxies (Ciambur & Graham 2016) (red dots) and the MW (Ciambur et al. 2017) compared with the face-on peanuts in our simulated models. The symbols have the same meaning as in Fig. 12.

would be instructive to compare these with a bigger peanut galaxy sample in a future study, including more galaxies with face-on disks.

## 7. DISCUSSION AND CONCLUSIONS

We have addressed an important issue on the physical nature of boxy/peanut structures in local disk galaxies. The conventional view is that these structures form as a result of the vertical buckling instability of a bar (Combes & Sanders 1981). During this instability, stars are excited at the vertical inner Lindblad resonances (Pfenniger 1985; Pfenniger & Friedli 1991; Martinez-Valpuesta et al. 2006), resulting in a vertically puffed up bar with a characteristic peanut morphology, most prominent when the host galaxy’s disk is viewed in an edge-on projection. This special viewing angle restriction had resulted in a low number of galaxies observed with these peanuts, al-

though recently more and more disk galaxies are being reported to host such peanuts as near-(face-on) diagnostics are being identified (Méndez-Abreu et al. 2008; Iannuzzi & Athanassoula 2015; Erwin & Debattista 2016, 2017). In addition to the viewing angle restriction, there are other structural components in a disk galaxy that are known to contribute to the weakening of the bar and peanut structures intrinsically - they are mainly the gas component (Berentzen et al. 1998; Athanassoula et al. 2013) and the central mass concentrations (Hasan et al. 1993; Bournaud et al. 2005). Despite these, a number of observed galaxies have shown peanut signatures in face-on projection (Laurikainen et al. 2011; Erwin & Debattista 2013). So the actual reason why some galaxies reveal peanuts in face-on, remains to be investigated. Our simulations are purely collisionless, and hence are unable to comment on the impact of gas on the final appearance of the peanut structure. However, our simulations show it clearly that as the peanut structure in edge-on projection gets stronger, its face-on counterpart also becomes prominent (see, Sim1 evolution above).

In our simulations of cold stellar disks with low bulge-to-disk mass ratios, bars with strong three-dimensional peanut-shaped structures form. The results from our simulations show that there is a strong pinch along the bar-minor axis, giving it a peanut shape in the X-Y plane of the galaxy disk and this is *not* due to any projection effect, see Fig. 3 and Fig. 4. As expected, the pinch in the density is also accompanied by its signature in the kinematic map, see Fig. 14. Such a density-kinematic pinch is highly prominent in Sim1 and least in Sim3. Recently, Patsis & Katsanikas (2014) has reported possible orbital connection between the face-on and edge-on peanut morphology. However, the exact physical conditions that lead to the formation of these 3D X/peanut structures need further investigation.

It is important to distinguish our simulated face-on peanuts from barlenses. Barlenses are thought to have a dynamical connection with vertical ( $z$ -direction) boxy/peanut structures: as shown by Athanassoula et al. (2015), barlenses and boxy/peanut structures are essentially the same feature viewed at a different angle; further evidence is also found in observations (Herrera-Endoqui et al. 2017). In a similar fashion, barlenses and X-shaped features are also being compared by Laurikainen & Salo (2017). All three of our simulated models of galaxies host boxy/peanut/X-shaped structures when their disks are viewed edge-on *and* face-on. This is not due to any projection effect; there is a peanut both in edge-on and face-on projection - making this a truly three-dimensional peanut. In addition to the well-known cylindrical rotation when viewed edge-on, we found the signature of cylindrical rotation to extend even in low inclination angle, i.e., in near face-on projection. We have shown clear

cylindrical rotation in all the simulated 3D peanuts at  $30^\circ$  inclination from face-on.

Our primary conclusions from this work are:

1. Our simulations have revealed strong peanut structures associated with an ansae and an outer ring at the end of the bar — as seen in the galaxy IC 5240.

2. There is a close morphological resemblance between our simulations and IC 5240. The structural components (a classical Sérsic bulge with  $n \approx 1$ , a double exponential disk, a Ferrers bar, and a Gaussian ring/ansae) that were required to model the images of our three simulated galaxies and IC 5240 are the same, albeit with different parameter values. The broader ring in Sim2 required an additional Gaussian ring component.

3. Beyond the cutoff of the Peanut/X/bowtie structures, which have their maximum strength (relative to the galaxy light) at 0.5 times the length of the bar, and extend out towards the end of the bar, we discover a positive/negative feature in the  $B_6$  profile that is associated with the ansae/ring when the disk is viewed face-on.

4. The peanut-shaped structure appears to contribute little signal to the major-axis light profile; the decomposition of this profile does not require a peanut component in either the simulations or the real galaxy. We therefore consider it likely that some past works claiming to have found and measured the peanut-shaped structure arising from the bar, i.e. the ill-named "pseudobulge", via the decomposition of major-axis light profiles, have in fact not measured the galaxy's "pseudobulge", but have instead detected and measured the classical bulge.

5. We have found that in various structural and kinematic scaling diagrams (Figures 16, 13 16), the quantitative peanut parameters measured in our face-on simulated galaxies are in broad agreement with quantitative peanut parameters measured in real, relatively edge-on, galaxies.

6. With a near-face-on projection, there is a *kinematic pinch* along the bar minor axis — coinciding with the density pinch. Prominent cylindrical rotation is evident even in near face-on projection.

A.W.G. was supported under the Australian Research Council's funding scheme (DP17012923). We would like to thank the anonymous referee for useful comments. We would like to thank Ron Buta for pointing out IC 5240 as an example of a possible face-on peanut. All the simulations were performed at the IUCAA HPC centre.

## REFERENCES

- Athanassoula, E. 2005, MNRAS, 358, 1477  
 —. 2016, Galactic Bulges, 418, 391  
 Athanassoula, E., & Beaton, R. L. 2006, MNRAS, 370, 1499

- Athanassoula, E., Laurikainen, E., Salo, H., & Bosma, A. 2015, MNRAS, 454, 3843  
 Athanassoula, E., Machado, R. E. G., & Rodionov, S. A. 2013, MNRAS, 429, 1949  
 Athanassoula, E., & Misiriotis, A. 2002, MNRAS, 330, 35  
 Berentzen, I., Heller, C. H., Shlosman, I., & Fricke, K. J. 1998, MNRAS, 300, 49  
 Binney, J., & Tremaine, S. 1987, Galactic dynamics, ed. Binney, J. & Tremaine, S.  
 Block, D. L., Puerari, I., Knapen, J. H., et al. 2001, A&A, 375, 761  
 Bournaud, F., Combes, F., & Semelin, B. 2005, MNRAS, 364, L18  
 Bureau, M., & Freeman, K. C. 1999, AJ, 118, 126  
 Buta, R. 1995, ApJS, 96, 39  
 Buta, R., & Crocker, D. A. 1991, AJ, 102, 1715  
 Buta, R. J., Sheth, K., Regan, M., et al. 2010, ApJS, 190, 147  
 Chung, A., & Bureau, M. 2004, AJ, 127, 3192  
 Ciambur, B. C. 2015, ApJ, 810, 120  
 —. 2016, PASA, 33, e062  
 Ciambur, B. C., & Graham, A. W. 2016, MNRAS, 459, 1276  
 Ciambur, B. C., Graham, A. W., & Bland-Hawthorn, J. 2017, ArXiv e-prints  
 Combes, F. 2011, in IAU Symposium, Vol. 271, Astrophysical Dynamics: From Stars to Galaxies, ed. N. H. Brummell, A. S. Brun, M. S. Miesch, & Y. Ponty, 119–126  
 Combes, F. 2016, Galactic Bulges, 418, 413  
 Combes, F., Debbasch, F., Friedli, D., & Pfenniger, D. 1990, A&A, 233, 82  
 Combes, F., & Sanders, R. H. 1981, A&A, 96, 164  
 de Vaucouleurs, G., de Vaucouleurs, A., Corwin, Jr., H. G., et al. 1991, Third Reference Catalogue of Bright Galaxies. Volume I: Explanations and references. Volume II: Data for galaxies between  $0^h$  and  $12^h$ . Volume III: Data for galaxies between  $12^h$  and  $24^h$ .  
 Debattista, V. P., Carollo, C. M., Mayer, L., & Moore, B. 2005, ApJ, 628, 678  
 Debattista, V. P., Mayer, L., Carollo, C. M., et al. 2006, ApJ, 645, 209  
 Dwek, E., Arendt, R. G., Hauser, M. G., et al. 1995, ApJ, 445, 716  
 Elmegreen, B. G., Bournaud, F., & Elmegreen, D. M. 2008, ApJ, 688, 67  
 Erwin, P., & Debattista, V. P. 2013, MNRAS, 431, 3060  
 —. 2016, ApJ, 825, L30  
 —. 2017, MNRAS, 468, 2058  
 Evans, N. W. 1993, MNRAS, 260, 191  
 Graham, A. 2015, Highlights of Astronomy, 16, 360  
 Graham, A. W. 2014, in Astronomical Society of the Pacific Conference Series, Vol. 480, Structure and Dynamics of Disk Galaxies, ed. M. S. Seigar & P. Treuhardt, 185  
 Hasan, H., Pfenniger, D., & Norman, C. 1993, ApJ, 409, 91  
 Herrera-Endoqui, M., Salo, H., Laurikainen, E., & Knapen, J. H. 2017, A&A, 599, A43  
 Iannuzzi, F., & Athanassoula, E. 2015, MNRAS, 450, 2514  
 Jogee, S., Scoville, N., & Kenney, J. D. P. 2005, ApJ, 630, 837  
 King, I. R. 1966, AJ, 71, 64  
 Kuijken, K., & Dubinski, J. 1995, MNRAS, 277, 1341  
 Kuijken, K., & Merrifield, M. R. 1995, ApJ, 443, L13  
 Laurikainen, E., & Salo, H. 2017, A&A, 598, A10  
 Laurikainen, E., Salo, H., Athanassoula, E., Bosma, A., & Herrera-Endoqui, M. 2014, MNRAS, 444, L80  
 Laurikainen, E., Salo, H., Buta, R., & Knapen, J. H. 2011, MNRAS, 418, 1452  
 Laurikainen, E., Salo, H., Buta, R., & Vasylyev, S. 2004, MNRAS, 355, 1251  
 Lütticke, R., Dettmar, R.-J., & Pohlen, M. 2000a, A&AS, 145, 405

- . 2000b, *A&A*, 362, 435
- Martinez-Valpuesta, I., Knapen, J. H., & Buta, R. 2007, *AJ*, 134, 1863
- Martinez-Valpuesta, I., & Shlosman, I. 2004, *ApJ*, 613, L29
- Martinez-Valpuesta, I., Shlosman, I., & Heller, C. 2006, *ApJ*, 637, 214
- McMillan, P. J., & Dehnen, W. 2007, *MNRAS*, 378, 541
- Méndez-Abreu, J., Corsini, E. M., Debattista, V. P., et al. 2008, *ApJ*, 679, L73
- Mould, J. R., Huchra, J. P., Freedman, W. L., et al. 2000, *ApJ*, 529, 786
- O’Neill, J. K., & Dubinski, J. 2003, *MNRAS*, 346, 251
- Patsis, P. A., & Katsanikas, M. 2014, *MNRAS*, 445, 3546
- Patsis, P. A., Skokos, C., & Athanassoula, E. 2002, *MNRAS*, 337, 578
- Pfenniger, D. 1985, *A&A*, 150, 112
- Pfenniger, D., & Friedli, D. 1991, *A&A*, 252, 75
- Pfenniger, D., & Norman, C. 1990, *ApJ*, 363, 391
- Planck Collaboration, Ade, P. A. R., Aghanim, N., et al. 2016, *A&A*, 594, A13
- Quillen, A. C., Kuchinski, L. E., Frogel, J. A., & DePoy, D. L. 1997, *ApJ*, 481, 179
- Raha, N., Sellwood, J. A., James, R. A., & Kahn, F. D. 1991, *Nature*, 352, 411
- Saha, K., & Gerhard, O. 2013, *MNRAS*, 430, 2039
- Saha, K., Martinez-Valpuesta, I., & Gerhard, O. 2012, *MNRAS*, 421, 333
- Saha, K., Pfenniger, D., & Taam, R. E. 2013, *ApJ*, 764, 123
- Saha, K., Tseng, Y., & Taam, R. E. 2010, *ApJ*, 721, 1878
- Sellwood, J. A., & Carlberg, R. G. 2014, *ApJ*, 785, 137
- Sheth, K., Regan, M., Hinz, J. L., et al. 2010, *PASP*, 122, 1397
- Springel, V., Yoshida, N., & White, S. D. M. 2001, *NewA*, 6, 79
- Toomre, A. 1969, *ApJ*, 158, 899
- Williams, M. J., Zamojski, M. A., Bureau, M., et al. 2011, *MNRAS*, 414, 2163
- Yoshino, A., & Yamauchi, C. 2015, *MNRAS*, 446, 3749